A Low-Profile Broadband Circularly Polarized Patch Antenna Based on Characteristic Mode Analysis

Xi Gao, Guowei Tian, Zhaoyu Shou, and Simin Li

***Abstract*—A low-profile and broadband metasurface antenna is proposed for circular polarization radiation. The metasurface is an array of subwavelength square patches. The modal behaviors of the proposed metasurface are investigated by using the characteristic mode theory. Two characteristic modes with the same resonant frequencies and orthogonal current distributions are chosen as operation modes. Furthermore, a hybrid feed system consisting of a cross-slot and a microstrip line is employed to excite the two orthogonal modes having a 90° phase difference to obtain circular polarization radiation. Based on these concepts, an antenna with low profile of $0.07\lambda_0$(λ_0 is the free-space wavelength at an operation frequency of 5.5GHz) is designed. The measurement results show that the proposed antenna has −10 dB impedance bandwidth of 4.8–6.35 GHz and 3 dB axial-ratio bandwidth of 4.85–6 GHz. Moreover, the antenna gain is 6.8–9.7 dBic in the whole axial-ratio bandwidth.**

***Index Terms*—Broadband, characteristic mode, circular polarization, metasurface.**

I. Introduction

IN WIRELESS communication systems, circularly polarized (CP) antennas are independent of the transmitter and receiver orientation, and furthermore, they can also mitigate the multipath distortions and polarization mismatch losses. Therefore, CP antennas are essential in many applications such as handheld, portable devices, RFID, wireless/satellite communications, and sensor systems [1], [2]. As we know, the traditional single-feed CP microstrip antennas are simple in structure and easy to fabricate [3]–[6]. However, these antennas have a disadvantage of narrow bandwidth, which greatly limits their applications. To address these issues, researchers have proposed many methods. Adopting thick dielectric plates [7], multilayer patch structures [8], or using double-feed or multifeed networks [9] can effectively extend the bandwidth of CP antennas, but these methods increase the geometric dimension of antennas.

Metasurfaces are 2-D counterparts of metamaterials, which have been extensively utilized to improve the radiation performance of CP patch antennas [10]–[13]. In these applications, metasurfaces are usually used as a superstrate to broaden the bandwidth of antennas. For example, a 3 × 4 patch array was proposed to obtain wideband radiation in C-band satellite communication [10]. The 3 dB axial ratio (AR) bandwidth reaches 16.5% from 4.9 to 5.9 GHz. Again, a metasurface consisting of 4 × 4 periodic metal patches was used as a superstrate to expand the 3 dB AR bandwidth of a CP patch antenna [11]. In this antenna, the 3 dB AR bandwidth is 23.4% ranging from 4.9 to 6.2 GHz. In addition, metasurfaces were also employed as a substrate or reflector to enhance the impedance bandwidth of CP antennas. Agarwal *et al.* [12] designed an artificial magnetic conductor ground plane as back reflector to realize a low-profile and wideband CP antenna. These previous research works have demonstrated that metasurfaces can effectively broaden the bandwidth of CP antennas, but they have a disadvantage of low gain or high profile. Furthermore, the best antenna performance is realized by optimizing the whole antenna structure including the loaded metasurface, which complicates the design process of an antenna. In the optimization process, the antennas are usually looked as a "black box," and therefore, they cannot provide clear physical insight for antenna design.

In this letter, a low-profile, high gain, and broadband CP metasurface antenna is introduced. The modal currents and their radiation characteristics of the proposed metasruface are investigated by using characteristic mode (CM) theory [14]–[19]. Based on the CM analyses, two degenerated CMs with orthogonal current distributions are selected as operation modes to obtain CP radiation. Meanwhile, a single-feed structure composed of a microstrip meander line and a cross-slot is employed to simultaneously excite the two orthogonal modes with a 90° phase difference. The simulations and experimental results verify the CP radiation performance of the proposed antenna.

II. Antenna Configuration

The geometry of the proposed antenna is shown in Fig. 1. It is composed of three metallic layers and two dielectric layers, in which the two dielectric substrates are F4B with a relative dielectric constant of 3.5 and a loss tangent of 0.003. Fig. 1(a) presents the metallic metasurface layer, which is an array of subwavelength square patches with a width of w and an edge-to-edge distance of g. Fig. 1(b) presents the metal ground with cross-slot etched on its central location, and Fig. 1(c) shows the feed structure, which is a microstrip meander line under the cross-slot. The microwave energy is coupled from the microstrip line to the metasurface antenna by the cross-slot. The side view

Manuscript received October 6, 2020; revised December 2, 2020; accepted December 4, 2020. Date of publication December 14, 2020; date of current version February 3, 2021. This work was supported in part by the National Science Foundation of China under Grant 61761010 and in part by the Natural Science Foundation of Guangxi under Grant 2018GXNSFAA281193. *(Corresponding authors: Guowei Tian; Simin Li.)*

Xi Gao and Simin Li are with the School of Electrical and Information Engineering, Guangxi University of Science and Technology, Liuzhou 545006, China (e-mail: gao_xi76@163.com; siminl@guet.edu.cn).

Guowei Tian and Zhaoyu Shou are with the School of Information and Communication, Guilin University of Electronic Technology, Guilin 541004, China (e-mail: gw_tian@163.com; guilinshou@guet.edu.cn).

Digital Object Identifier 10.1109/LAWP.2020.3044320

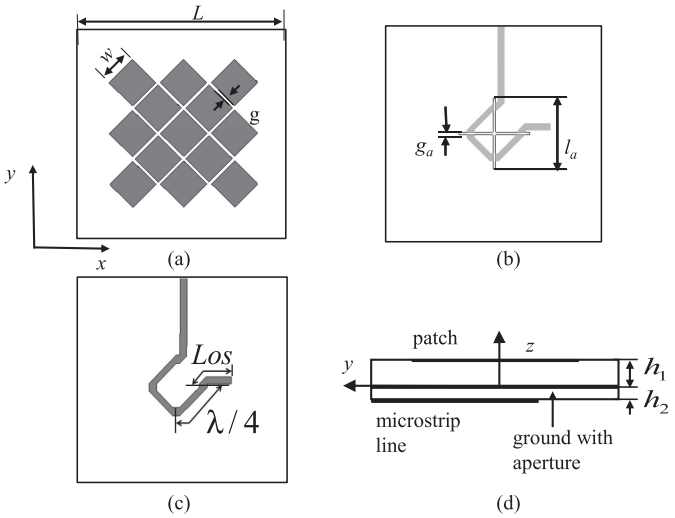

Fig. 1. Configuration of the metasurface-based antenna. (a) Top view of metasurface. (b) Top view of metal ground on which a cross-slot is etched. (c) Back view of microstrip line. (d) Side view of the proposed antenna.

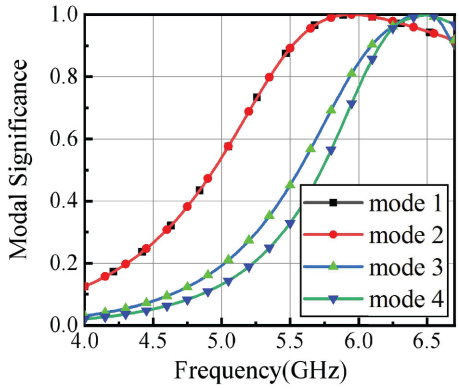

Fig. 2. MS values for the first four modes.

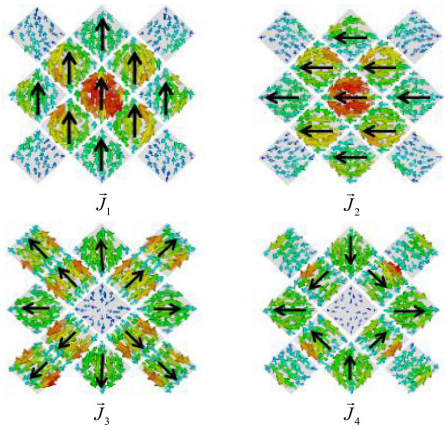

Fig. 3. Current distributions for $\vec{J}_1$ and $\vec{J}_2$ at 6 GHz, and for $\vec{J}_3$ and $\vec{J}_4$ at 6.5 GHz.

of the antenna is presented in Fig. 1(d). Here, the metasurface layer has the same configuration as that in [18], but they operate on different CMs. In this letter, two orthogonal resonant modes are selected as operation modes. As long as the two orthogonal resonant modes are simultaneously excited and have a 90° phase difference, the CP radiation can be generated.

III. Mechanism of the Metasurface Antenna

A. Theory of Characteristic Mode

In CM theory, the modal behavior is described by the generalized eigenvalue equation $X\vec{J}_n = \lambda_n R\vec{J}_n$, where $\vec{J}_n$ represents the characteristic current or eigenvector for mode n, and λ_n is the eigenvalue. Take note that the total current ($\vec{J}$) on the perfect electric conductor (PEC) can be expressed as $\vec{J} = \sum C_n \vec{J}_n$, where C_n is a complex modal expansion coefficient, which determines the weight of each mode. The modal significance ($\mathrm{MS} = |1/(1 + j\lambda_n)|$) is an important parameter, which is used to analyze the intrinsic radiation characteristic of a structure. When MS $= 1$, it implies that the mode is in resonant state and radiates with maximum efficiency, while when MS ≈ 0, it corresponds to the mode hardly resonating or radiating.

B. Characteristic Mode Analysis of Metasurface

Based on the above theory, we first simulate the MS of the metasurface by using the commercial software CST 2016. Fig. 2 presents the MS of the first four characteristic modes. As can be seen, $\vec{J}_1$ and $\vec{J}_2$ have identical MS values. Furthermore, the MS values are equal to 1 at 5.9 GHz, showing that the modes $\vec{J}_1$ and $\vec{J}_2$ resonate at this frequency. The modes $\vec{J}_3$ and $\vec{J}_4$ share the same trend of variation against frequency, but they have the same resonant frequency of 6.5 GHz. In all the four modes, all have their resonant frequencies; hence, each mode can be employed as an operation mode of antenna if an adaptive feed is employed to excite it.

In order to further characterize the radiation performance of the metasurface, we present the modal currents of the first four modes, as shown in Fig. 3. The modal current $\vec{J}_1$ is in-phase across the entire metasurface and is polarized in the y-direction. For $\vec{J}_2$, it has an identical current distribution to $\vec{J}_1$ except the 90° phase difference. Moreover, $\vec{J}_1$ and $\vec{J}_2$ have the same MS value (see Fig. 2); hence, they are a pair of degenerate modes. The modal currents $\vec{J}_3$ and $\vec{J}_4$ are both self-symmetrical about x- and y-axes. Fig. 4 presents the far-field patterns of the first four modes. It is clearly observed that $\vec{J}_1$ and $\vec{J}_2$ have the same far-field patterns, but they have orthogonal polarization states due to their orthogonal surface current distributions. For $\vec{J}_3$ and $\vec{J}_4$, their far-field radiation patterns appear null at a central position because of their out-of-phase current distributions. According to the surface current distributions of $\vec{J}_1$ and $\vec{J}_2$ and their far-field patterns, we deduce that a circular polarization radiation can be obtained if the two modes are simultaneously excited with a 90° phase difference. Therefore, the modes $\vec{J}_1$ and $\vec{J}_2$ are selected as candidates for generating circular polarization radiation.

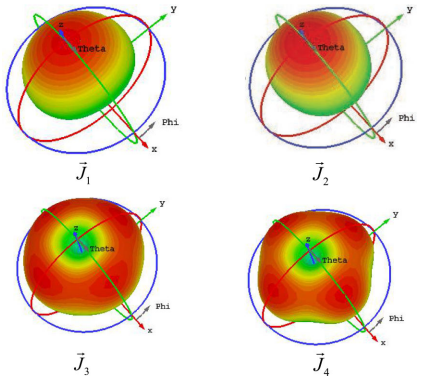

Fig. 4. Far-field patterns for $\vec{J}_1$ and $\vec{J}_2$ at 6 GHz, and for $\vec{J}_3$ and $\vec{J}_4$ at 6.5 GHz.

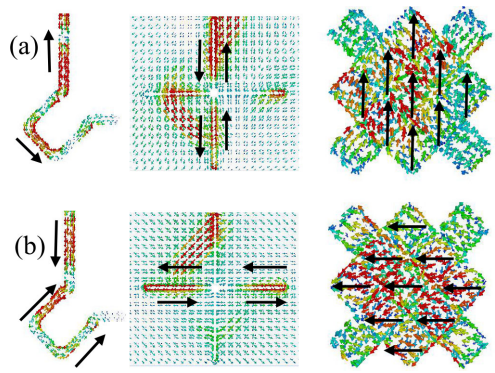

Fig. 5. Current distributions on microstrip line, cross-slot, and metasurface from different phases of excitation signal. (a) $\varphi = 0°$. (b) $\varphi = 90°$.

C. Antenna Feeding Network

To obtain circular polarization radiation, an adaptive feed network should be employed to simultaneously excite $\vec{J}_1$ and $\vec{J}_2$ and to generate a 90° phase difference between them. From Fig. 3, we find that maximum values of $\vec{J}_1$ and $\vec{J}_2$ concentrate at the central patch, and the submaximal currents distribute at the surrounding patches. For $\vec{J}_3$ and $\vec{J}_4$, however, they present completely different current distributions. At the central patch, the current is very weak, and the maximum current appears at the four corner patches. Based on these characteristics of current distribution, the feed structure should be positioned under the center patch of the metasurface, so that $\vec{J}_1$ and $\vec{J}_2$ can be excited efficiently, while $\vec{J}_3$ and $\vec{J}_4$ are difficult to be excited. To meet this condition, we employ a single-feed network that is a combination of a cross-slot and a microstrip meander-line to excite the antenna [4], as presented in Fig. 1(b) and (c).

To investigate the operation mechanism of the feed system in detail, we simulate the current distributions on the microstrip line, on cross-slot, and on metasurface antenna for different phases of excitation signal ($\varphi = 0°$ and $\varphi = 90°$). Fig. 5 presents the simulated results, in which Figs. 5(a) and (b) correspond to $\varphi = 0°$ and $\varphi = 90°$, respectively. For $\varphi = 0°$, the current on the microstrip line distributes as a standing wave state [see the left part in Fig. 5(a)], and the standing waves effectively excite the cross-slot [see the middle part in Fig. 5(a)]. In this case,

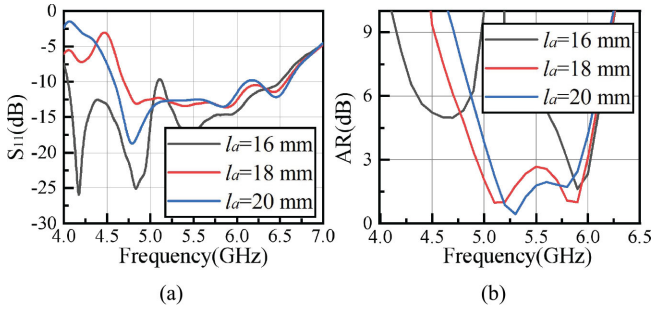

Fig. 6. Simulated (a) S_{11} and (b) AR for different la.

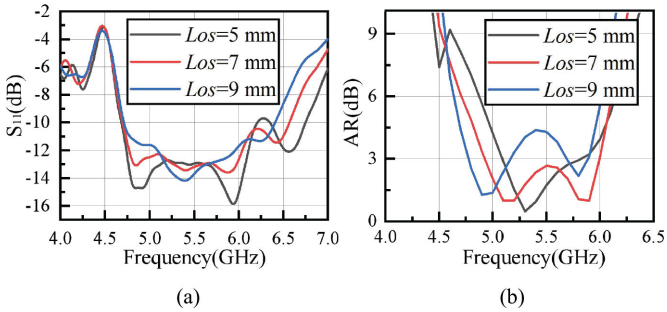

Fig. 7. Simulated (a) S_{11} and (b) AR for different Los.

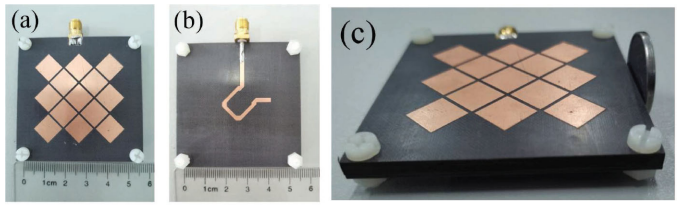

Fig. 8. Fabricated prototype of the proposed metasurface antenna. (a) Top view. (b) Back view. (c) Side view.

the currents mainly concentrate on the vertical arm, and the horizontal arm has weak current distribution due to the 90° phase difference with the vertical arm. The currents on the vertical arm further excite the modal current $\vec{J}_1$ of the metasurface [see the right part in Fig. 5(a)]. Similarly, for $\varphi = 90°$, the modal current $\vec{J}_2$ of metasurface is effectively excited, as presented in Fig. 5(b). As a result, a circular polarization radiation is formed.

Figs. 6 and 7 present the influences of slot length (l_a) and microstrip line length (Los) on S-parameters and ARs. It can be seen that the largest -10 dB impedance bandwidth and 3 dB AR bandwidth can be achieved by properly adjusting the parameters l_a and Los. The final optimized parameters are set as $L = 55$ mm, $w = 8.7$ mm, $g = 0.8$ mm, $l_a = 18$ mm, $g_a = 0.7$ mm, $h_1 = 3$ mm, $h_2 = 0.8$ mm, and $Los = 7$ mm.

IV. Simulation and Experimental Results

To demonstrate the performance of the proposed antenna, we fabricated a sample and measured its S-parameter and radiation performance. Fig. 8 presents the prototype of the fabricated

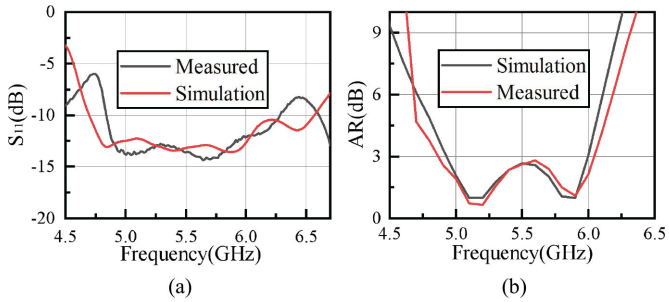

Fig. 9. (a) *S*-parameters. (b) AR of the antenna.

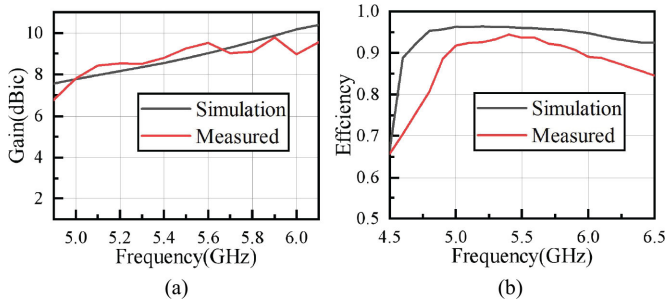

Fig. 10. (a) Gains and (b) efficiency of the antenna.

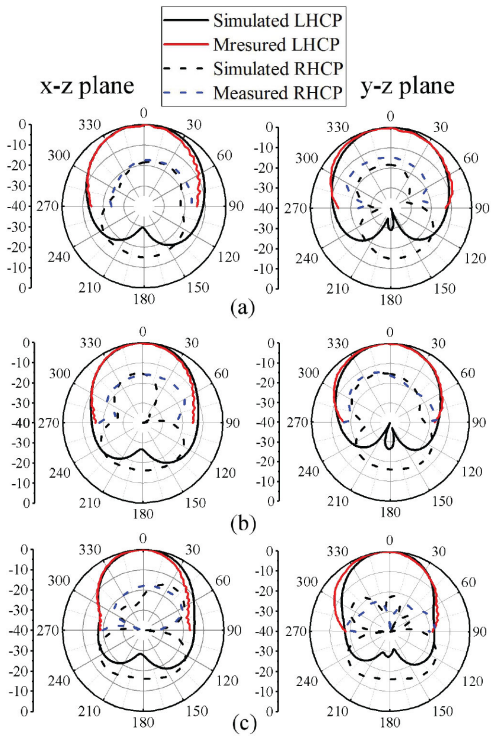

Fig. 11. Normalized radiation patterns in *xoz* (left side) and *yoz* (right side) planes at (a) 5, (b) 5.5, and (c) 5.9 GHz.

sample. The measured and simulated *S*-parameters and ARs are compared in Fig. 9. The measured results have good agreement with the simulations. As shown in Fig. 9(a), the measured impedance bandwidth for $S_{11} < -10$ dB is 28.2% (4.8–6.35 GHz), which is slightly lesser than the simulated results of 33.6% (4.7–6.6 GHz). This difference may be caused by the fabrication and measurement tolerances. Fig. 9(b) presents the simulated and measured 3 dB AR bandwidth, which reveals that the simulated 3 dB AR bandwidth is in the frequency range of 4.9–6 GHz, and the measured bandwidth ranges from 4.85 to 6 GHz. Fig. 10(a) shows the simulated and measured antenna gains varying as frequency. In the operation frequency band, the simulated and measured gains range from 7.6 to 10.2 dBic and from 6.8 to 9.7 dBic, respectively. As shown in Fig. 10(b), the measurement efficiency is higher than 88% throughout the 3 dB AR bandwidth, which is slightly lesser than that of simulations.

The simulated and measured far-field radiation patterns in both the *xoy* plane and *yoz* plane at 5 GHz, 5.5, and 5.9 GHz are plotted in Fig. 11. It is noted that the forward radiation is only measured due to the limitation of our measurement system. There is good agreement between the measured and simulated results. The radiation is left-hand CP (LHCP), and right-hand CP (RHCP) is cross polarization. The cross-polarization level is lower than −18 dB. Additionally, the radiation patterns possess good symmetry, implying that the feed system excites the high-purity CMs ($\vec{J}_1$ and $\vec{J}_2$) revealed in CM analysis.

Table I shows the comparison of the proposed antenna and other reported CP patch antennas. Comparing with [10] and [16], our proposed antenna has a wider 3 dB AR bandwidth. On the other hand, the designed antenna occupies the highest gain except that its 3 dB AR bandwidth is slightly lesser than those of the antennas in [11] and [12]. In general, our design presents good overall performance, such as low profile, high gain, and wide bandwidth.

TABLE I
COMPARISON OF THE PROPOSED ANTENNA WITH REFERENCE ANTENNA

Ref	Size(λ^3)	Frequency (GHz)	Impedance Bandwidth	3dB ARBW	Peak gain (dBic)
[3]	0.76*0.76*0.1	2.53	13%	8.7%	7.3
[10]	0.6*0.49*0.07	5.25	33.7%	16.5%	5.8
[11]	0.58*0.58*0.056	5.5	45.6%	23.4%	7.6
[12]	0.72*0.60*0.19	6	36.67%	23.3%	7
[16]	1.4*1.4*0.07	5.6	38.8%	14.3%	8.5
This work	1*1*0.07	5.5	28.2%	20.9%	9.7

V. CONCLUSION

We presented a low profile, high gain, and broadband CP metasurface antenna. By investigating the mode behaviors of metasurface, two orthogonal modes are employed as operation modes. Meanwhile, a feed network composed of a microstrip meander line and a cross-slot was proposed to simultaneously excite the two orthogonal modes, and furthermore, a 90° phase difference was generated between them, resulting in a circular polarization radiation. We also fabricated a sample to experimentally verify the performance of the CP antenna. Both the experimental results and numerical simulations reveal that the proposed antenna has advantages of low profile, high gain, and wide bandwidth including impedance bandwidth and 3 dB AR bandwidth. The designed antenna has good applications in wireless communications.

REFERENCES

[1] Y. F. Lin, Y. K. Wang, H. M. Chen, and Z. Z. Yang, "Circularly polarized crossed dipole antenna with phase delay lines for RFID handheld reader," *IEEE Trans. Antennas Propag.*, vol. 60, no. 3, pp. 1221–1227, Mar. 2012.

[2] B. R. Rao, W. Kunysz, R. Fante, and K. McDonald, *GPS/GNSS Antennas*. Norwood, MA, USA: Artech House, 2013.

[3] T. N. Chang, J. M. Lin, and Y. G. Chen, "A circularly polarized ring-antenna fed by a serially coupled square slot-ring," *IEEE Trans. Antennas Propag.*, vol. 60, no. 2, pp. 1132–1135, Feb. 2012.

[4] H. Kim, B. M. Lee, and Y. J. Yoon, "A single-feeding circularly polarized microstrip antenna with the effect of hybrid feeding," *IEEE Antennas Wireless Propag. Lett.*, vol. 2, pp. 74–77, 2003.

[5] K. L. Wong and J. Y. Wu, "Single-feed small circularly polarised square microstrip antenna," *Electron. Lett,* vol. 33, no. 22, pp. 1833–1834, Oct. 1997.

[6] H. D. Chen and W. S. Chen, "Probe-fed compact circular microstrip antenna for circular polarization," *Microw. Opt. Technol. Lett.*, vol. 29, no. 1, pp. 52–54, 2001.

[7] J. Kovitz and Y. Rahmat-Samii, "Using thick substrates and capacitive probe compensation to enhance the bandwidth of traditional CP patch antennas," *IEEE Trans. Antennas Propag.*, vol. 62, no. 10, pp. 4970–4979, Oct. 2014.

[8] N. Nasimuddin, K. P. Esselle, and A. K. Verma, "Wideband circularly polarized stacked microstrip antennas," *IEEE Antennas Wireless Propag. Lett.*, vol. 6, pp. 21–24, 2007.

[9] S. D. Targonski and D. M. Pozar, "Design of wideband circularly polarized aperture-coupled microstrip antennas," *IEEE Trans. Antennas Propag.*, vol. 41, no. 2, pp. 214–220, Feb. 1993.

[10] Z. Wu, L. Li, Y. J. Li, and X. Chen, "Metasurface superstrate antenna with wideband circular polarization for satellite communication application," *IEEE Antennas Wireless Propag. Lett.*, vol. 15, pp. 374–377, 2016.

[11] S. X. Ta and I. Park, "Low-profile broadband circularly polarized patch antenna using metasurface," *IEEE Trans. Antennas Propag.*, vol. 63, no. 12, pp. 5929–5934, Dec. 2015.

[12] K. Agarwal, Nasimuddin, and A. Alphones, "Unidirectional wideband circularly polarised aperture antennas backed with artificial magnetic conductor reflectors," *Microw., Antennas Propag,* vol. 7, no. 5, pp. 338–346, Apr. 2013.

[13] K. Agarwal, Nasimuddin, and A. Alphones, "Wideband circularly polarized AMC reflector backed aperture antenna," *IEEE Trans. Antennas Propag.*, vol. 61, no. 3, pp. 1456–1461, Mar. 2013.

[14] R. Harrington and J. Mautz, "Theory of characteristic modes for conducting bodies," *IEEE Trans. Antennas Propag.*, vol. AP-19, no. 5, pp. 622–628, Sep. 1971.

[15] M. Meng and N. Nie, "Study on characteristic mode analysis of three-dimensional conducting objects in lossless layered medium," *IEEE Access*, vol. 6, pp. 77606–77614, 2018.

[16] C. Zhao and C. F. Wang, "Characteristic mode design of wide band circularly polarized patch antenna consisting of H-shaped unit cells," *IEEE Access*, vol. 6, pp. 25292–25299, 2018.

[17] F. H. Lin and Z. N. Chen, "A method of suppressing higher-order modes for improving radiation performance of metasurface multiport antennas using characteristic mode analysis," *IEEE Trans. Antennas Propag.*, vol. 66, no. 4, pp. 1894–1902, Apr. 2018.

[18] F. H. Lin and Z. N. Chen, "Low-profile wideband metasurface antennas using characteristic mode analysis," *IEEE Trans. Antennas Propag.*, vol. 65, no. 4, pp. 1706–1713, Apr. 2017.

[19] T. Li and Z. N. Chen, "A dual-band metasurface antenna using characteristic mode analysis," *IEEE Trans. Antennas Propag.*, vol. 66, no. 10, pp. 5620–5624, Oct. 2018.